



**FINITE ELEMENT MODEL OF THE CYLINDRICAL GEM DETECTOR
AS NEW INNER TRACKER OF Kloe2
AND
MECHANICAL CHARACTERIZATION OF THE EMPLOYED MATERIALS**

L. Quintieri, G. Bencivenni, D. Domenici, A. Ceccarelli,
S. Cerioni, S. Lauciani, M. Pistilli
INFN, Laboratori Nazionali di Frascati, P.O. Box 13, I-00044 Frascati, Italy

Abstract

In this report we describe the study we have done to characterize the mechanics of the GEM cylindrical detector to be used as new inner tracker for the Kloe2 experiment. First of all we needed to describe accurately the mechanical behavior of the non conventional materials used for the different cylindrical layers. So that, in the first part of the report, the measurements of the tensile tests, that we did to define the mechanical properties of the used material, are accurately described. At the end of the experimental tests, we were able to derive the Elasticity Modulus values for the material of which each cylinder is made and accurately reconstruct the correspondent $\sigma(\epsilon)$ curves.

These experimental values have been used (in the input database for Ansys code) to perform 3-D simulations of the linear and non-linear structural response of the detector under several tensile loads, in order to estimate the entity of the consequently induced strain and stress.

One of the main objectives of this work, in fact, consists in the realization of a valuable computational tool that allows to foresee and analyze the mechanical response of the GEM detector to specified loads once boundary conditions are set. In order to be confident in the reliability of the simulation results, a validation against experimental well-know configurations has been done. The comparison between the finite element code predictions for the GEM detector prototype with the experimental results is discussed.

1 The new inner tracker based on GEM technology: conceptual design

Particle detectors based on GEM technology offer several advantages, the most important being: low mass, fully cylindrical and dead-zone-free. GEM-based detector is studied at the LNF as future inner tracker for the KLOE experiment at the DAFNE Φ -factory. A cylindrical GEM detector will be composed by five concentric cylinders made of thin (from 50 to 100 μm thick) kapton foils: the cathode, the three GEMs and the Anode. The final result is a very light detector. The built prototype has been show in figure 1

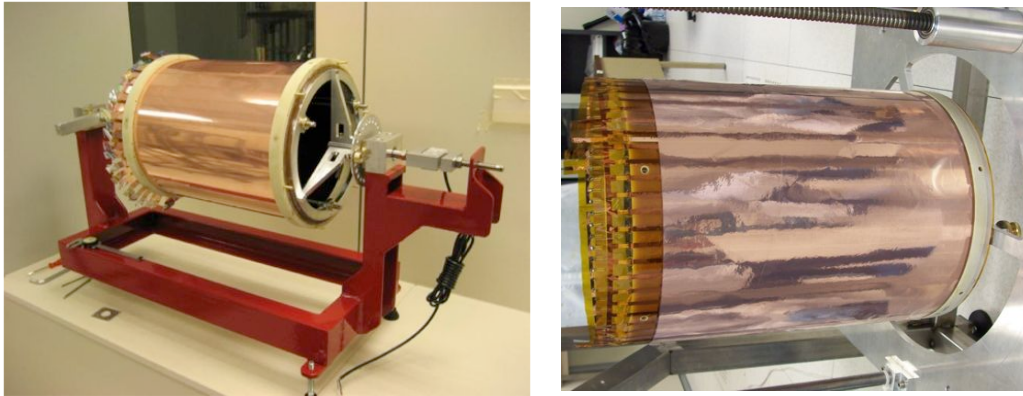


Figure 1: The full assembled prototype (mounted on the tensile test machine, on the left); the prototype during assemblage, on the right.

In order to acquire the necessary know-how, namely on mechanics, readout and front-end electronics, for the construction of the final detector a full scale prototype has been designed and built in all details.

The aim of the work described in this report is the analysis and study of the mechanical behavior of the GEM cylindrical detector. The final goal is to be able to estimate the deformations of the detector when loads and boundary condition are well known. To achieve this objective, as first task, it is necessary to characterize the material behavior of each component: for this reason the “ $\sigma(\epsilon)$ ” curve for the different involved materials has been obtained by an extensive campaign of experimental measurements at the mechanical workshop of the LNF laboratory.

These data have been recorded, suitably elaborated and finally they have been properly inserted in the finite element model of the prototype, realized by Ansys code, as explained later in this report.

2 The cylindrical prototype: description of the mechanical design

The full prototype detector is composed of 5 concentric cylinders, that are respectively described in the following items:

- Anode: the external cylinder. It has an inner diameter of 318 mm and a thickness of $110\mu\text{m}$. It is composed of an external layer of $5\mu\text{m}$ of copper on both sides and an inner core made of uniform kapton foil ($100\mu\text{m}$). The main mechanical properties of the kapton sheets are reported in table 1. These data have been taken from the

Kapton Sheet' mechanical Properties

Density (kg/m ³)	Young [GPa]	Poisson -	Tensile Strength, Yield [MPa]	Tensile Strength, Ultimate [MPa]
1420	2.5	0.34	69	231

Table 1: Kapton Main Mechanical Properties

“DuPont” catalogue [1] and are valid for kapton films whose thickness goes from 25 to $125\mu\text{m}$. The values reported in the table refer to standard temperature. More complete information can be found on the the cited catalogue.

- GEMs: the middle cylinders. They have an inner diameter that goes from 314 mm (the larger one) to 306 mm (the inner one) and a thickness of $60\mu\text{m}$. They are composed of an external layer of $5\mu\text{m}$ on both sides and an inner core made of kapton foil ($50\mu\text{m}$). On the contrary of Anode and Catode, these foils have conic holes distributed regularly according an horizontal and vertical pitch of $140\mu\text{m}$. The transversal shape of the holes has been shown in schematic way in figure 2, together with a picture of the tissue obtained with the electronic optic microscope.
- Catode: the inner cylinder. It has an inner diameter of 300 mm and a thickness of $105\mu\text{m}$. It is composed of only one copper layer of $5\mu\text{m}$ on one side and of a uniform kapton foil $100\mu\text{m}$ thick, on the other.

The total length of the cylinders is 452 mm, even if the active length is only that inside the permaglass rings (that is 358, as shown in figure 3). These rings, of about 25 mm height, are located at the extremities of the assembly in order to keep in shape the cylinders and to constitute the interface for supporting.

The mechanical properties of the permaglass have been summarized in table 2. Permaglass has been chosen, essentially, because: it has good insulating electrical properties, it is a sufficiently light material but with suitable rigidity. Each cylindrical foils is fixed

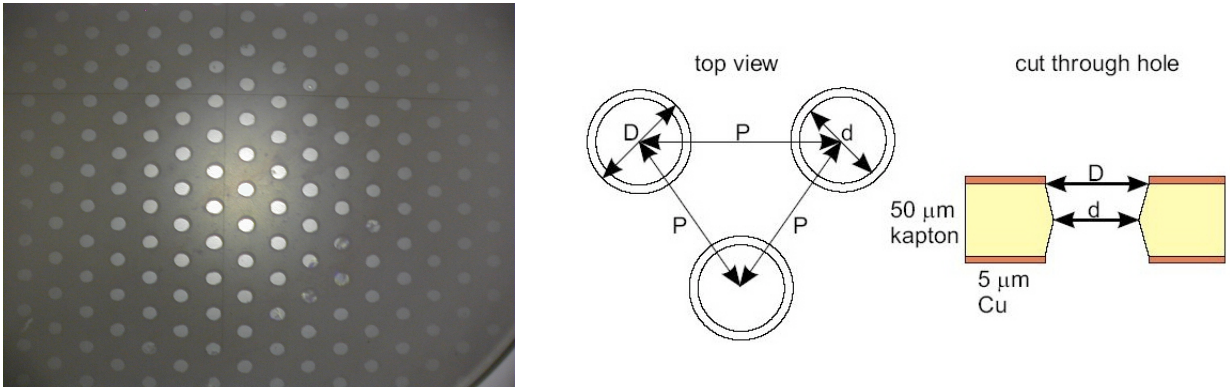


Figure 2: On the left: picture of the hole matrix of a GEM foil made by a profile projector instrument with a factor magnification equal to 50; on the right, geometrical description of the hole matrix.

between two concentric permaglass rings, using a special Epoxy glue (an Araldite 2011), as shown in the simplified scheme of figure 3.

Density kg/m ³	Young [GPa]	Poisson	Tensile Strength [MPa]
1850	24	0.3	300

Table 2: Permaglas' EPC 203 mechanical properties

3 Characterization of the materials

One of the main task of this work regards the correct characterization of the structural behavior of the materials involved in the detector construction. An accurate mathematical description of the stress-strain curve has to be suitably derived and introduced in the Ansys code for constructing the finite element model of the detector.

As we have already specified, the GEM cylinder is made of a thin insulating polymer foil (kapton in the specific case), coated on both sides with a very thin metal layer (copper). Kapton exhibits a visco-plastic¹ behavior and the mechanical properties are strongly affected by the final shape in which it is worked for usage. In particular, extremely thin films show a mechanical behavior that is not directly deducible from that of the bulk material. Moreover the thin layers of copper coating and the ordered matrix of conic holes of the inner GEM foils could affect the structural behavior of the overall sheet.

¹Unlike purely elastic substances, a viscoelastic substance has an elastic component and a viscous component. Viscoelastic materials exhibit time dependent strain and a brittle like mechanical behavior.

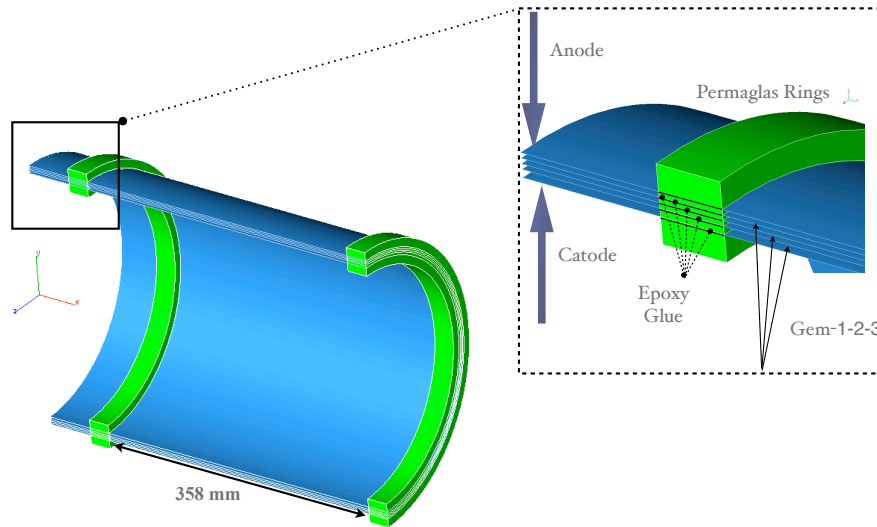


Figure 3: A simplified scheme of half prototype: the cylindrical layers are fixed on the permaglass rings by a very thin layer of epoxy glue

Taking all this into account, we cannot use the mechanic elastic properties (as young modulus or yield and ultimate tensile strength) available in literature for Kapton and assume these to be also the GEM foil mechanical properties, but we are obliged to characterize the mechanical behavior of the GEM, Anode and Catode sheets by suitable tests.

The quantitative effect that the geometrical shape and multilayer composition could have on the mechanical properties has been derived by dedicated tests. whose results of these measurements are reported in the following paragraphs.

3.1 Tesile tests on GEM, Anode and Catode sheets

The machine used for characterizing the mechanical behavior of the GEM sheets is a “Tenso Test 5000”. It is located at the workshop of the LNF Technical Division (Metrology Department). It is an electro-mechanic computerized machine used for tensile, compression and flexural tests. In figure 4 a tensile test on a suitable conformed sheet is shown in two phases: while the increasing load is applied and after the specimen break down.

In case of polymeric material as kapton, the stress to failure could be influenced by the load speed application. In the performed tests, this factor has not been taken into account, as the GEM detector has supposed to be gradually pre-tensioned, avoiding suddenly change both in load intensity and direction.

The GEM-cylinders are foreseen to work under static tensile load to minimize the

transversal deformations that the gravitational and electric field could cause, affecting consequently the cylindrical symmetry. In this frame, a creep deformation study could be interesting, as it could occur as a result of long term exposure also to levels of stress that are well below the yield strength of the material. In fact an important consequence of the viscoelasticity of polymers is that their deformations under stress are time dependent. If the imposed mechanical stress is held constant, then the resultant strain will increase with time. The study of the creep effect will constitute the next step of our work that wants to achieve a knowledge and characterization of the GEM detector mechanical behavior as complete as possible.



Figure 4: Tensile test on a specimen: during load application on the left and after break down, on the right.

3.2 Elaboration of the experimental data

Several curves (Force F vs Elongation ΔL) have been collected for each material. In order to derive the unique stress-strain curve, $\sigma(\epsilon)$, this approach for managing and elaborating the raw data has been applied:

- From the tables of value $[F, \Delta L]$ provided by the tensile test machine, we derived the corresponding σ , dividing the F values by the transversal cross section of the sheet. Because the sheet has essentially a brittle behavior, the cross section does not change significantly during the test, so that we can use the initial value of the cross section up to the collapse. The deformation ϵ has been estimated as $(\Delta L - \Delta L_{cor})/L_0$, where ΔL_{cor} is the correction factor that has to be applied in all those cases in which the tensile machine records an elongation value different from zero even for $F=0$ N (it corresponds to the offset value $\Delta L[F = 0]$). In such a way we make the $\sigma(\epsilon)$ curve effectively passing by the origin (0,0) as it should be.

- We averaged all the measured stress values for a fixed elongation value. In order to perform this properly we used the Matlab software (see appendix 1). The raw data are made of different numbers of point $(F, \Delta L)$ that are taken at not regular intervals of the applied force. We divided the elongation range² in 100 parts ($\Delta\epsilon_i = Range/100; \epsilon_i = (n - 1) * \Delta\epsilon_i, n = 1, 2..100$) and we averaged arithmetically the values of the different sets of data falling in each subinterval. The estimated mean value was assigned to the deformation value (ϵ_i) corresponding to the center of the selected subinterval.
- We assumed to have a conservative approach with respect to the ultimate stress. This means that we decided to extend the $\sigma(\epsilon)$ curve up to the lower break point registered in the raw data sets.
- Since the statistics for every material is poor (no more than 6 sets of raw data) we cannot estimate a significant statistical error.

The averaged final curves $\sigma(\epsilon)$ for the material used for Anode, Catode and GEM cylinders respectively have been reconstructed and are discussed in details in the following.

3.2.1 *Experimental Results for Anode sheets*

The Anode cylinder is made of a not perforated kapton foil that has been coated on both sides with extremely thin copper layer ($5 \mu\text{m}$). It has a mass of about 100 g and an inner diameter of 318 mm ($110 \mu\text{m}$ thickness).

In figure 5 the elementary rectangular strips used for characterising the material behaviour are shown after rupture. The tested sheets are rectangular strips of 280 mm length, 25mm width with a cross section of 3.25 mm^2 (thickness 0.13 mm). The measurements that we describe in this report and that we use for properly setting the mechanical properties of the used foils have been taken in July 2008.

Five tests have been performed, with only one test rejected. The force-elongation plot for all the successful tests and the deduced stress-strain deformation curves “ $\sigma(\epsilon)$ ” are reported in figures 6 and 7, respectively . The analysis of the data allows to conclude, regarding the material of which the Anode is made, that:

1. It exhibits a brittle behavior: it means that it does not have a yield point clearly distinguishable and does not strain-harden because of plastic deformation. Consequently we only identified the ultimate strength, as that for which the structural failure of the specimens is reached. In order to individuate the yield point, the

²The shorter one of all set of data, to be conservative.



Figure 5: Anode specimens after tensile tests.

specimens should be unloaded periodically: after the yield stress the slope of the unloading lines should give the Young modulus in the respective region. In order to complete the mechanical characterization of the material, we have already planned a new suitable measurement campaign to identify, more precisely, the plastic deformation region (that is the region in which a permanent deformation is caused, even if the load is brought to zero), but it has to point out that there are no reasons to make the prototype to work in partial plasticity condition³.

2. A region of hookean behavior is distinguishable at low strains: an initial Young (Elasticity Modulus) value of 3.375 GPa has been estimated to represent the elastic behavior for low stress (up to $\sigma_{el} = 40MPa$, that corresponds to an elastic deformation of $\epsilon_{el} = 1.16\%$). This implies that the cylinder moves surely in the elastic region up to a tensile load value of about 4 kN, applied uniformly on the transversal cross section of the Anode cylinder. In the elastic region, the strain and stress in the cylinder are deducible by the Hook relation $\sigma = E_0\epsilon$, with $E_0 = 3.375$ GPa).
3. The ultimate tensile stress for the Anode material has been estimated to be 146 MPa with an expected elongation at break of 32.5 % (see figure 7). This means

³The tensile load is applied in order to minimize the transversal deformation due to gravity and electrostatic attraction to guarantee the right gap between concentric cylinders.

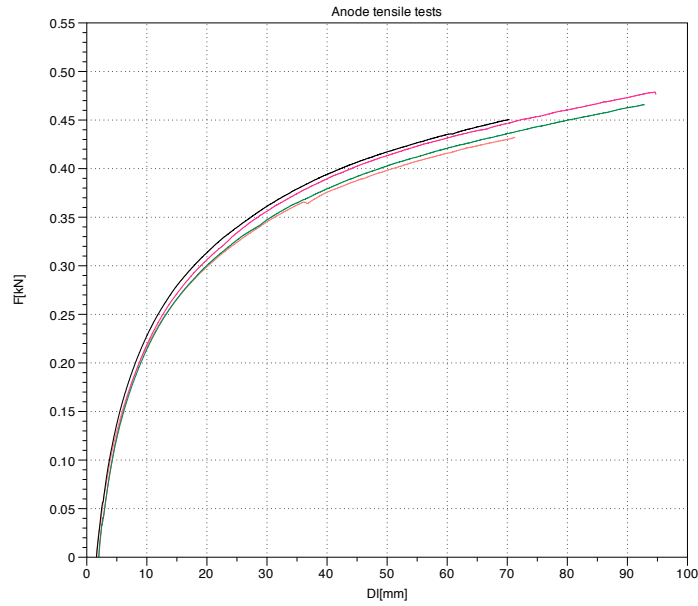


Figure 6: Experimental data for Anode specimens: force applied on the specimens vs total elongation.

that a uniformly distributed (on the circumference) tensile load ⁴ of about 16 kN is expected to cause the structural collapse of the Anode cylinder.

3.2.2 Experimental Results for Catode sheets

The Catode cylinder is made of a uniform kapton foil coated on only one side by a very thin copper layer ($5\mu\text{m}$). It has a mass of about 75 gr and an inner diameter of 300 mm (with an overall thickness of $105\mu\text{m}$). In figure 8 the specimens after break are shown.

The dimensions of the rectangular specimens used for the tensile tests are: 248 mm length, 24.50 mm width and transversal cross section equal to 2.45 mm^2 . Four tests have been successful performed and the results have been reported in figure 9, where the experimental data are shown in the force-elongation plot, while the derived stress-strain, $\sigma(\epsilon)$ curve, is reported on figure 10.

Elaborating the experimental data we can derive the following main informations on the mechanical behavior for the Catode material:

1. It also exhibits a brittle behavior: a linear region has been determined even if a yield stress point could be not assessed on the basis of these measurements, but, as

⁴ $F_{ult} = \sigma_{ult} * 2 * \pi * R_{cat} * t_{cat}$, where $t_{cat} = 110\mu\text{m}$

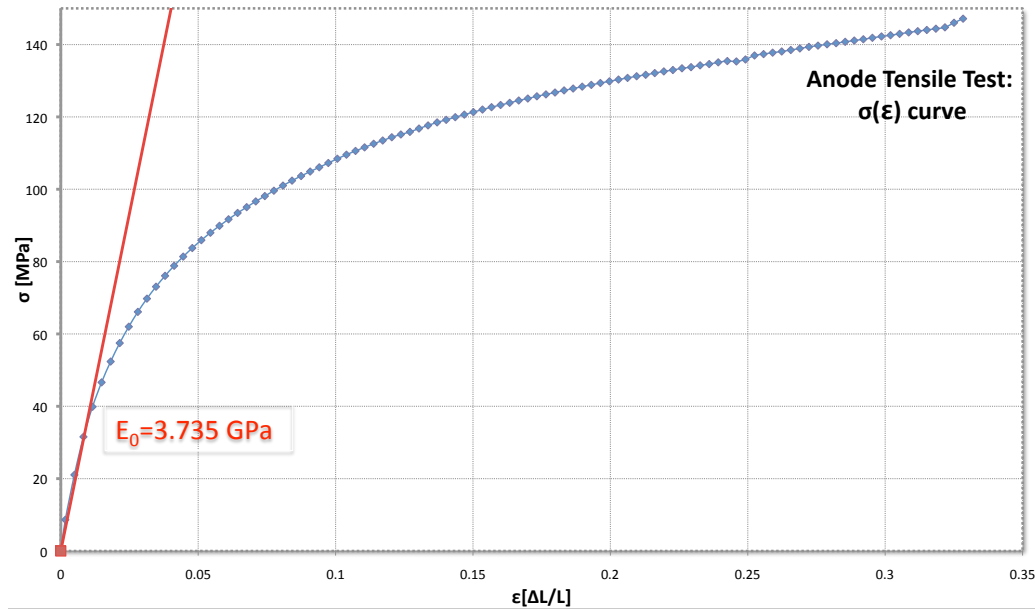


Figure 7: Derived curve Stress-Strain for Anode material.

already specified, loading-unloading cycles are necessary.

2. A region of linear behavior is distinguishable at low strains: an initial Young (Elasticity Modulus) value of 5.29 GPa has been estimated to represent the elastic behavior for low stress: the foil is elastic up to a strain of 0.7% that corresponds to a stress value of 33.5 MPa. So that an elastic behavior is assured if we apply loads not greater than about 3.3 kN. In the elastic region, the strain and stress in the cylinder are deducible by the Hook relation $\sigma = E_0 \epsilon$, with $E_0 = 5.29$ GPa.
3. The ultimate tensile stress for the Catode material has been estimated to be $\sigma_{ult} = 134$ MPa with an expected elongation at break of 15.7 % (see figure 10). This means that the mechanical failure of the cylinder is expected to arrive for load greater than 14 kN, having supposed the cylinder to be simply stretched by an axial load uniformly distributed on the circumference.

3.2.3 Experimental Results for GEM sheets

GEM foils are made of perforated kapton inner foils (50 μm , see paragraph §2), coated on both sides by a copper layer, for an overall foil thickness of 60 μm . The GEM cylinders in the prototype have almost the same mass of about 68 g (with little difference, of the

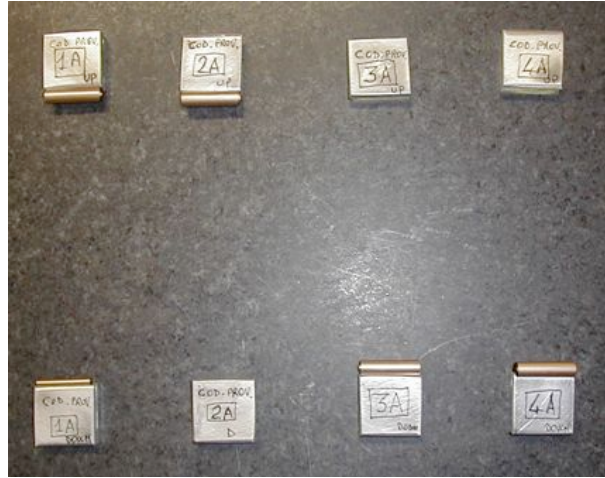


Figure 8: Catode specimens after tensile tests.

order of tenths of grams, from the smaller to the larger ones). Figure 11 shows the 4 GEM specimens after testing.

The experimental data collected during the testing are reported on the right in figure 11, where the force-displacement plots for every specimen are shown. The derived $\sigma(\epsilon)$ curve of figure 12 describes the mechanical behavior of the material of which the GEM cylinders are made. The mechanical behavior of the GEM foils deduced from the experimental data can be summarized in the following items:

1. The same considerations of item 1 of paragraphs §3.2.1 and §3.2.2 are also valid for GEM material.
2. A region of linear behavior is distinguishable at low strains: the foil is elastic up to a strain of 0.4% with a $\sigma_{el}(0.4\%) = 33.5\text{MPa}$, that corresponds consequently to an estimated initial Young (Elasticity Modulus) value of 4.8 GPa. In the elastic region, the strain and stress in the material are related by the Hook relation $\sigma = E_0\epsilon$, with $E_0 = 4.8\text{ GPa}$. These experimental results imply that the GEM cylinders of the prototype are expected to exhibit elastic behavior when the applied tensile load is below 1kN (for sake of precision the following values have been calculated: 0.98 kN for the inner GEM cylinder, 0.99 kN for the middle one and 1.0 kN for the external cylinder).
3. The ultimate tensile stress for the GEM material has been estimated to be $\sigma_{ult} = 76\text{MPa}$ with an expected elongation at break of 9.2 % (see figure 10). This means

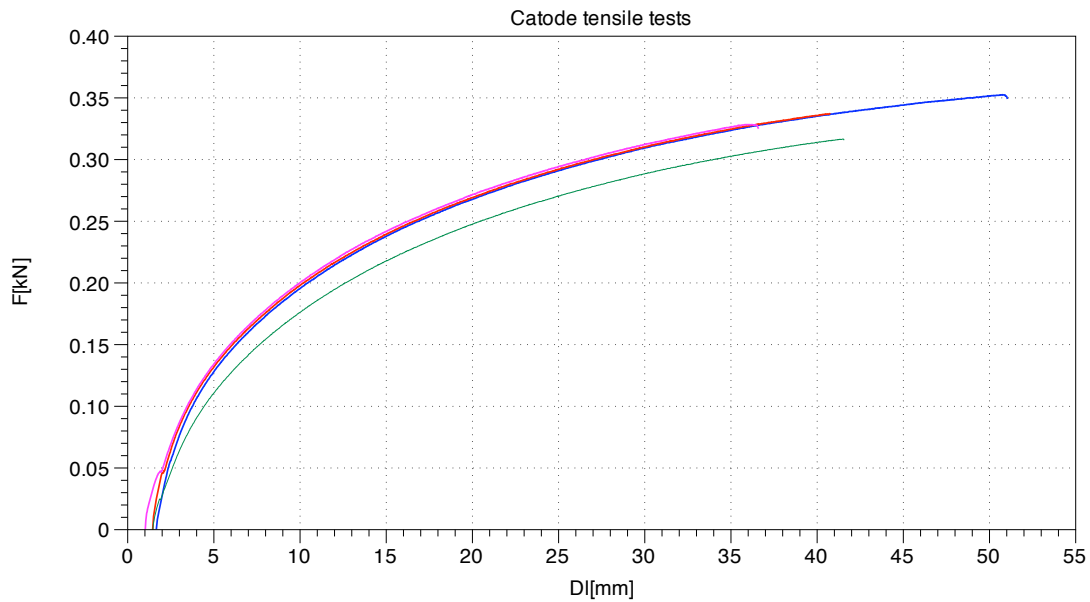


Figure 9: Experimental data for Catode specimens: force applied on the specimens vs total elongation.

that the mechanical failure of the GEM cylinders is caused by tensile load greater than 4 kN (namely the calculated value are respectively: 4.3 kN for the inner GEM cylinder, 4.44 kN for the middle one and 4.5 kN for the external cylinder).

3.2.4 Experimental Results for simply Kapton sheets: check of measurement reliability

Several tensile tests have been done also for kapton specimens. The used specimens are rectangular strips: 280 mm length, 25 mm width and transversal cross section equal to 1.38 mm^2 (thickness=0.06 mm). In figure 13 the kapton strips after break are shown.

The experimental data have allowed to estimate the initial tensile elasticity modulus to be 3.1 GPa, while the estimated break elongation and the ultimate stress are respectively 24.2% and 145 MPa. The value of the initial Young Modulus is almost in agreement with the experimental values that could be found in literature or provided by several kapton film manufacturer: i.e. the tensile modulus declared by the DuPont Company for kapton polyamide film (100 HN Film, 25x150mm, $50 \mu\text{m}$ thick) is 2.5 GPa, that is about 24% lower with respect to the value we found. We have to stress that while the Young Modulus is independent of film thickness, the yield stress depends strongly on it[2]. The ultimate stress estimated in our tests is much lower (about 37 % less) than that (231 MPa) officially declared in the manufacturer catalogue or in the mat-web site: this could be due to

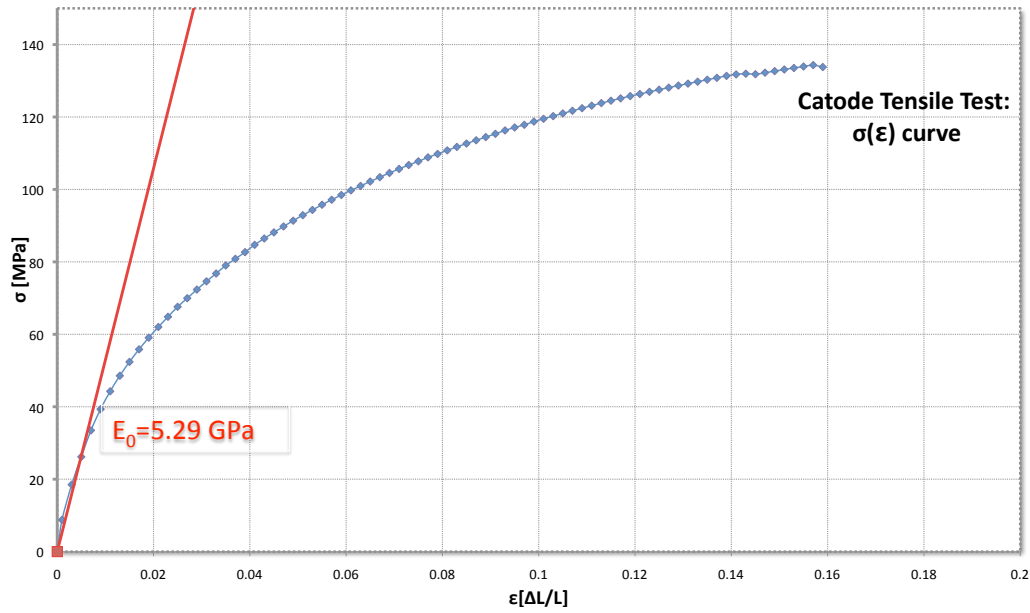


Figure 10: Derived curve Stress-Strain for Catode material.

the speed of load applications (faster than should be, in our measurements) or to the fact we have not properly prepared the specimen shape. We are going to investigate in more detail these differences. In any case, we certainly know that tensile properties may vary with specimen method of preparation, speed of testing, type of grips used and manner of measuring extension. Consequently, if very precise comparative results are desired, these factors must be carefully controlled. The official values given by the DuPont Manufacturer have been derived following the ASTM D-0882-91, Method A procedures. We think that the reason for which our tested kapton films seem to be more rigid should mainly due to the speed of load application. We are going to acquire and apply the complete ASTM procedure before repeating the tests, for further investigations.

4 The Finite Element Model

The finite element model of the prototype has been realized using the last version of Ansys code (Ansys11.0[3]). This model is intended to be used for evaluating the mechanical answer of the GEM detector in terms of deformations as a function of the applied loads and boundary constrains. The need to use finite element method to calculate stress and strain fields is essentially due to the complexity of the geometry and several important issues related to non linearities concerning structural behavior, as we are going to explain

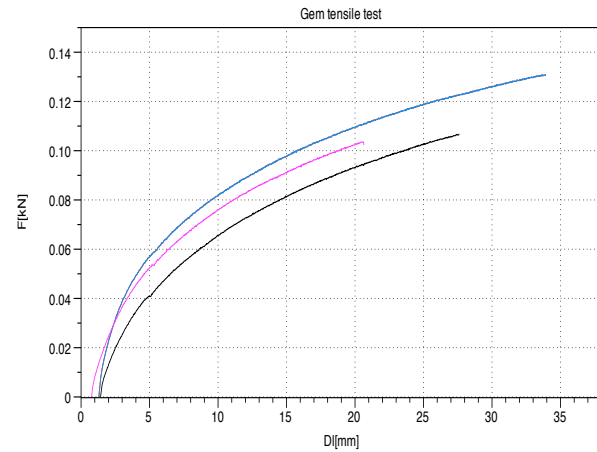


Figure 11: On the right: experimental data for GEM specimens: force applied on the specimens vs total elongation; On the left: GEM specimens after tests.

in what follows.

The aim is to have a tool that allows to foresee the mechanical response of the GEM detector when loads and boundary conditions are specified. In order to be confident in the reliability of the simulations results, a validation against experimental well-know configurations (that means measured deformations induced by well known load in specified boundary constraints) is required.

The main steps and guidelines followed in the development and check of the finite element model have been:

1. Adequate Geometrical Schematization. The important main features of the prototype design have been preserved, neglecting all those secondary details that should not affect the mechanical answer in our analysis (as for example holes in the permaglass rings. Since we are not interested in estimating stress in the permaglass rings, the presence of the holes has been taken into account just for performing a correct evaluation of the mass). This has been done for avoiding to loose time both in phase of construction and implementation of the model and in the simulation runtime.
2. Accurate mathematical description of the structural behavior of all the used materials. The material properties determined from measurements have been introduced as tables into database input for ANSYS. This has been done, even if the GEM detector is expected to work in linear region (that is in low stress and strain region), where only the initial young value in the curve $\sigma(\epsilon)$ is sufficient for describing the correct behavior.
3. Adequate choice of the kind of elements by which the geometrical domain has to

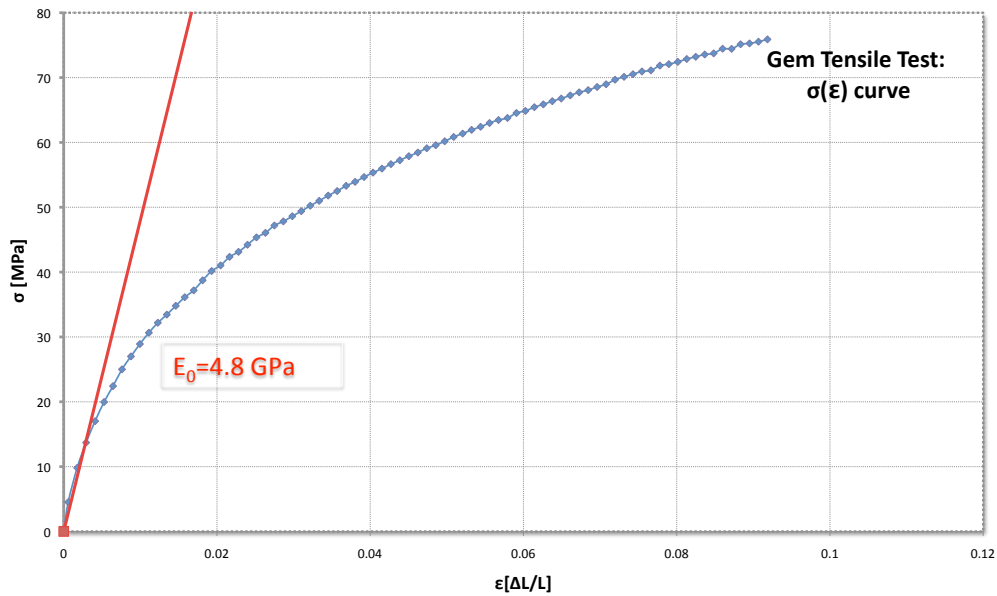


Figure 12: Derived stress-strain curve for GEM material.

be discretized. This is an important aspect that strongly affects the consistency and correctness of the calculated solutions. Different elements are used for meshing area or volumes, and the choice is based essentially on the mechanical rigidity is expected they exhibit. Moreover the choice is complicated by the fact that the elements to be used for our model in Ansys code should allow to simulate a non linear structural behavior either because of the entity of deformations or because of the non linear $\sigma(\epsilon)$ curve.

4. Realistic introduction of loads and boundary constraints (both external and internal ones, as those concerning the interface between different components.)
5. Identification of the kind of analysis (linear or non linear Structural Analysis, Modal Analysis, etc) and of the right algorithm for the solution estimation and CPU time optimization.
6. Final finite element model validation by comparison between the calculated deformations and the experimental values.

4.1 Geometry Schematization and Material Description: the Ansys Model

In figure 14 the solid model of the GEM detector realized in Ansys is reported. The

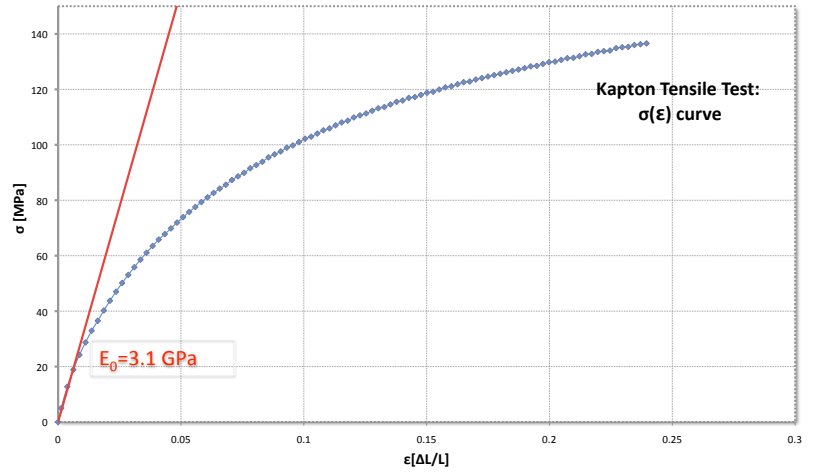


Figure 13: Kapton specimens after tensile tests, on the left; Derived kapton stress-strain curve on the right

Anode, Catode and GEM cylinders are modeled as area entities while the permaglass rings as volume ones (see figure 15). In table 3 several important parameters of the GEM detector model have been reported.

GEM Detector Ansys Model

Component	Inner Radius [m]	Thikness [μm]	Equivalent density[kg/m ³]	Linear El. Modulus [GPa]	Poisson Coefficient
Catode	0.150	100(Kap)+5(Cu)	1779	5.29	0.34
GEM-1	0.153	50(Kap)+10(Cu)	2291	4.8	0.335
GEM-2	0.155	50(Kap)+10(Cu)	2291	4.8	0.335
GEM-3	0.157	50(Kap)+10(Cu)	2291	4.8	0.335
Anode	0.159	100(Kap)+10(Cu)	2105	3.735	0.34

Table 3: Main geometric and material parameters

Each multi-layered foils (as that of Anode, Catode and GEMs) have been represented in the structural model as a unique foil of uniform material, taking care of preserving the effective mass and the real overall thickness. This has required to define and assign fictitious values for densities, that have been estimated according the following

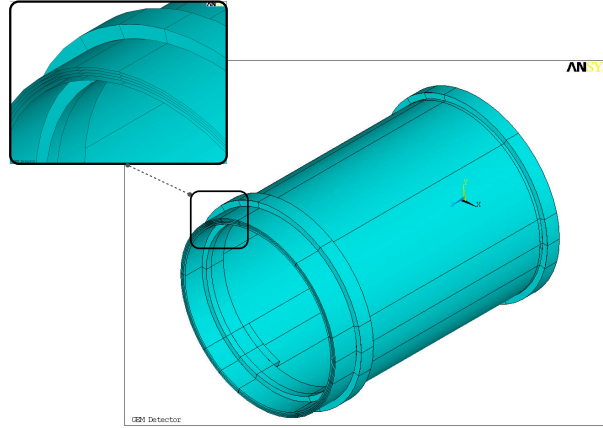


Figure 14:

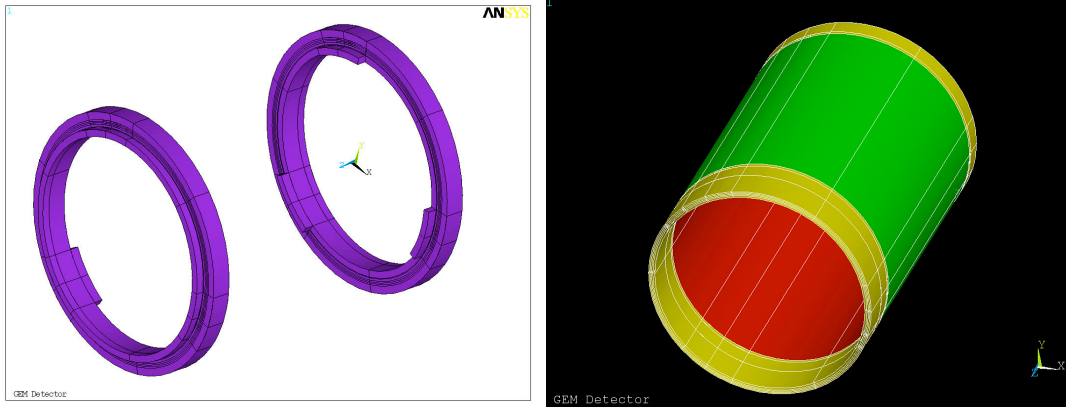


Figure 15: Volume entities in the model on the left (permaglass ring and brass plates); area entities on the right (different colors stay for different material).

expressions for the Catode, Anode and GEM foils, respectively:

$$\begin{aligned}
 \text{Catode} & : \rho_{\text{Catode}} = \left(\frac{h_{\text{cu}}\rho_{\text{kaptan}} + h_{\text{kaptan}}\rho_{\text{kaptan}}}{h_{\text{cu}} + h_{\text{kaptan}}} \right) \\
 \text{Anode} & : \rho_{\text{Anode}} = \left(\frac{2h_{\text{cu}}\rho_{\text{kaptan}} + h_{\text{kaptan}}\rho_{\text{kaptan}}}{2h_{\text{cu}} + h_{\text{kaptan}}} \right) \\
 \text{GEM} & : \rho_{\text{GEM}} = \left(\frac{2h_{\text{cu-rid}}\rho_{\text{kaptan-rid}} + h_{\text{kaptan}}\rho_{\text{kaptan-rid}}}{2h_{\text{cu-rid}} + h_{\text{kaptan-rid}}} \right)
 \end{aligned}$$

where $h_{\text{kaptan}} = h_{\text{kaptan}} = 100\mu\text{m}$, $h_{\text{kaptan}} = 50\mu\text{m}$, $\rho_{\text{cu}} = 8960 \text{ kg/m}^3$; $\rho_{\text{kaptan}} = 1420 \text{ kg/m}^3$. Finally $\rho_{\text{cu-rid}}$ and $\rho_{\text{kaptan-rid}}$ are the densities of, respectively, the perforated copper and kapton foil, estimated to be 14.4%⁵ lower than the uniform ones.

⁵The percentage of reduction respect to copper and kapton densities have been deduced according the

In table 4, the measured and estimated mass for the Anode and the external GEM cylinders have been compared, showing a very good agreement (error less than 5%), making us confident in having well represented the GEM-detector also from the point of view of the involved masses.

GEM Detector Ansys Model: Estimated and Measured Masses

Component	Estimated[g]	Measured[g]	Error [%]
Catode	83	-	-
Gem-3	68.5	68	(0.7%
Anode	101	105.	5%

Table 4: Check for masses in the finite element model

4.2 Model Meshing

After having assigned materials to the different solid regions, suitable elements have been chosen for discretization. Figure 16 shows the overall finite element model of the detector.

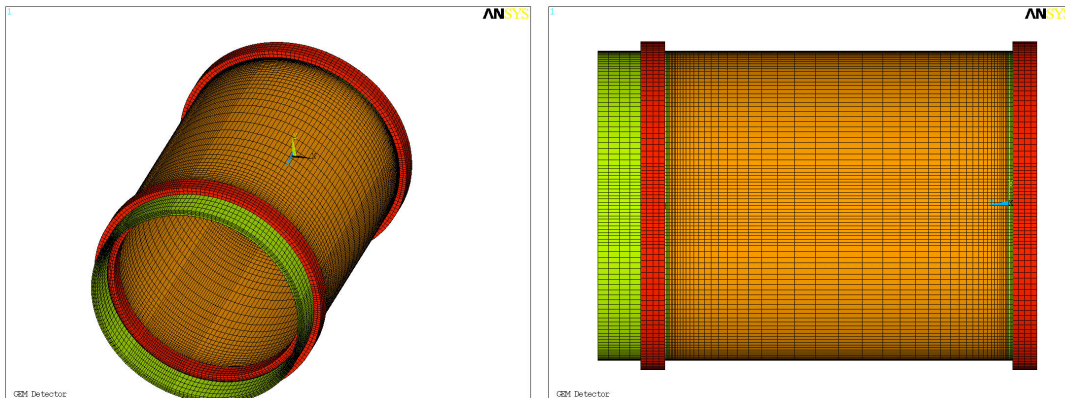


Figure 16: Finite Element Model: Mesh

The volumes and areas have been discretized by structured mapped mesh. In such a way we made the mesh finer in those regions where major stress and strain gradients are expected. Moreover the element size is crucial as well as the time step for the convergence in non linear calculations. Using a mapped mesh we can manage and optimize more accurately the size of the elements. In particular the number of elements per unit length along the cylinder generatrices is higher in the 5 mm strips of only kapton near the permaglass rings (inner side) on each cylinder (see figure 17), where high stress and strain gradients are expected. This has been done because sudden change of rigidity (as hole matrix geometry, shown in figure 2).

it happens for example, from 4.8 GPa of the copper double side to 3.1 GPa of the only kapton zone, in the GEM cylinders) could cause a concentration of stress and strain as it has been confirmed by the simulation results.

The choice of the kind of element depends on the kind of analysis we want to do and on the kind of detail of material structural behavior we want to introduce in the simulation as we explain in the following. For meshing volumes, either “solid45” or, alternatively, “solid95” brick elements could be used, as well “shell43” or “shell93” could be chosen for meshing areas.

“Solid45” elements are used for three-dimensional modeling of solid structures. The element is defined by eight nodes having three degrees of freedom at each node: translation in the nodal x, y, and z directions. This element has creep, swelling, stress stiffening, large deflection, and large strain capabilities. “Solid95” is a higher order version with respect to “solid45”, so that it is more suitable to mesh curved boundaries. Anyway the most important feature that Solid45 offers respect to 95, concerning our case, is that it allows to simulate non linear material, by introducing into suitable tables at least 100 points of the the stress-strain curve, $\sigma(\epsilon)$.

“Shell43” (with 4 nodes) is well suited to model linear, warped, moderately thick shell structures. In spite, “shell93” element has 8 node and it is particularly well suited to mesh curved shells: it has quadratic deformation shapes both in-plane directions. Both elements have six degrees of freedom at each node: translations in the nodal x, y, and z directions and rotations about the nodal x, y, and z-axes. They have plasticity, stress stiffening, large deflection, and large strain capabilities and in-plane and normal loads are permitted. Both of them can be chosen to simulate non linear material properties, providing option for this scope.

Simulations in linear field have been made with both the couple solid45/shell43 and solid95/shell93 and the results have been compared. In case of low applied loads responsible only of elastic deformation, the results obtained from the two different models (the one using solid45/shell63 and the other one using solid95/shell93) are perfectly in agreement, as expected for and as it should be.

We estimated that, at least, tensile loads greater than 6 kN are needed in order to generate in the whole structure stresses above 33.5 MPa, corresponding to the values for which GEM sheets enter in the non linear part of the $\sigma(\epsilon)$ curve (40 MPa is the corresponding value for Anode). We compared the results of linear and non linear analyses for loads up to about 5 kN and they agree very well. Instead for load greater than 6kN we performed non-linear calculations only.

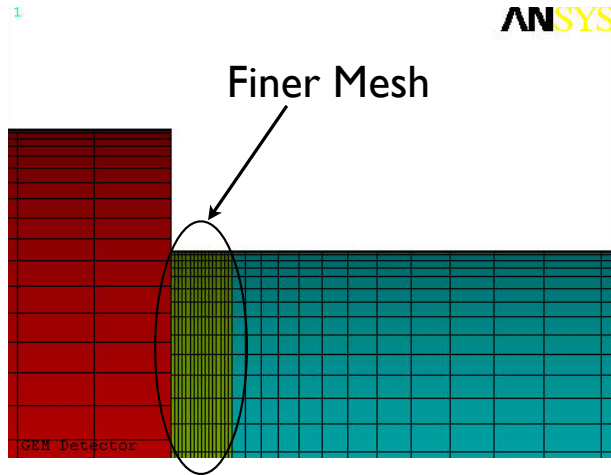


Figure 17: A detail of the cylinder mesh near the permaglass rings

4.2.1 Non-linearities in Geometry and Structural behavior of the Material

The prototype, that we want to characterize from the mechanical point of view, could have a non linear structural response because of non linearities related either to the geometry of its components or to the material behavior of which these components are made or contemporarily to both of these aspects. In fact the five cylinders have a thickness three order of magnitude less than the other dimensions (length and radius) and very low rigidity in transversal direction. As a consequence, elastic models based on the assumption of small deformation respect to the thickness could be no more valid to evaluate stress and strain. For this reason we must take into account the possibility to have large deformation, that implies a non linear static analysis.

Furthermore, the material itself, of which the cylinders are made, exhibits a non linear behavior or a multilinear one, due to the elasticity modulus gradually changing along the stress-strain curve. This requires the real “ $\sigma(\epsilon)$ ” curve to be properly inserted in the model, to estimate correctly the mechanical response of the GEM-detector when the applied loads are high enough to leave the narrow initial linear region.

The real $\sigma(\epsilon)$ curve has been introduced for Anode, Catode and GEM cylinders, using the command “TB,MELAS,mat,Ntemp,Npoints”. For the moment, values at standard temperature only have been provided and the analysis of the mechanical behavior as a function of the temperature has been planned as further advancement step of our study.

5 Validation of the FE model: Boundary and Load conditions in the simulations of the tensile tests

A special machine has been designed and realized for assembling and supporting the detector and also to equip it with electronic instrumentation. In figure 18 a cad of this machine is shown, whereas a picture of the full prototype mounted on the supporting machine is reported in figure 19.

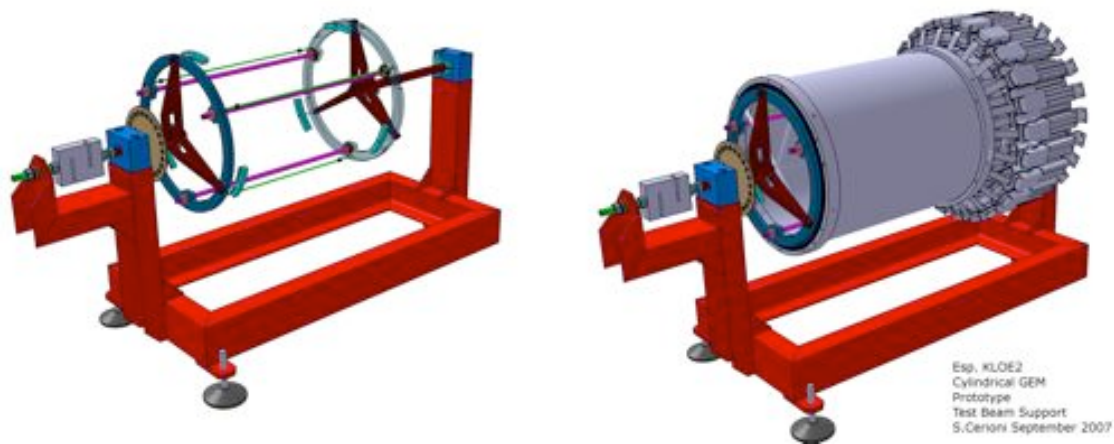


Figure 18: 3D cad of the machine for supporting and tensioning the detector on the left and 3D view of the detector mounted on the machine on the right.

Once properly assembled, the full prototype has been tested on a suitable Tensile Machine, at the mechanical Enea Workshop in Frascati. These tensile tests have been reputed to be a mandatory step in order to acquire a deep understanding of the proper way to use the finite element model to make correct predictions and to estimate how accurate the simulation results could be.

The machine used for testing is an INSTRON 5500 R, by which we can apply loads up to 100 kN in one way or cyclic modes. In figure 20 we can see in which manner the detector has been transported and prepared to be mounted on the ENEA Tensile machine: each permaglass ring is bolted on an aluminum ring that is rigidly connected to a stainless steel rod by three slabs at 120° .

Figure 21 shows the detector during the mounting phase on the Tensile machine, while figure 22 shows the extensometer (10 mm length) thanks to which we could estimate the elongation in between the two permaglass rings. In fact, the total crosshead displacement of the tensile machine is not representative of the detector deformation, including in it also the contribution of the elongation of the two stainless steel rods.

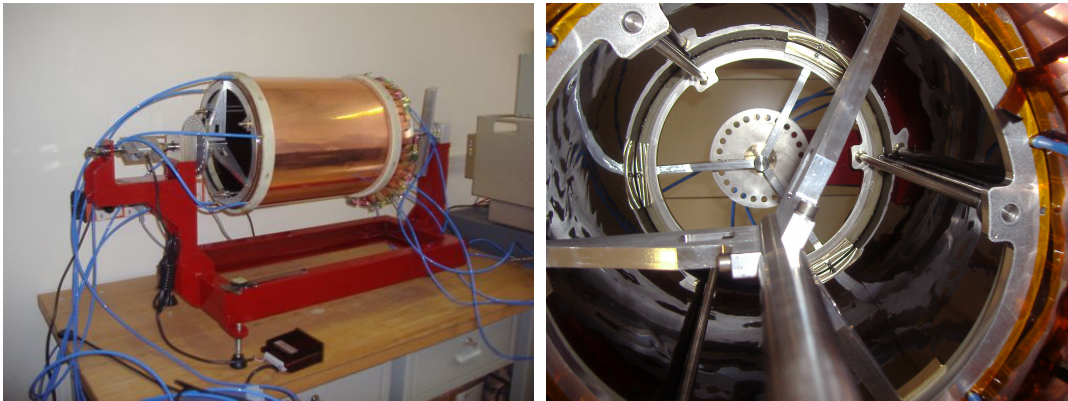


Figure 19: Detector prototype mounted on the tensile machine on the left. A detail of the inner part of the detector while mounted on the tensile machine.

Since we are interested in studying the answer of the detector in the stress-strain initial linear region, a maximum load of 3 kN was applied: this allows to measure the initial overall tensile modulus. A test speed of 0.4 mm/min has been applied, according the ASTM recommendations (it must be lower than 1 mm/min to properly measure the Young Modulus in thin plastic films).

5.1 Description of the Ansys Model for the tensile tests of the whole assembly

Our first simulations refer to the experimental set-up of the tensile tests, since the initial tasks of of this work consists in the validation of the overall finite element model, against the measured response, determined by the tensile tests.

The boundary conditions and the applied loads that we have introduced into the Ansys simulations to reproduce the tensile tests are described in what follows.

Concerning the constraints, in the finite element model, only one of the two permaglass rings is clumped, while the other one is free to move in the vertical direction, reproducing in such a way the real constraints during the test: only the lower aluminum bar is pulled downward, while the upper part is fixed. In the mathematical model this means that the nodes of the fixed permaglass rings (included the merged ones of the shell elements) have all the degrees of freedom suppressed. Moreover, on all the nodes of the solid/shell interface, the relative rotation have been suppressed. Finally, on the nodes of the permaglass ring, in contact with the aluminum ring that is free to move axially, only the axial translation “ U_z ” has been permitted (actually, in the tensile test configuration, the detector can only be elongated along the axis).

In figure 23 it is shown how the loads have been applied on the model. The axial force is applied as normal pressure distributed on those nodes of the free permaglass ring



Figure 20: Some details on the appendices used to mount the detector on the tensile machine

that are in contact with the brass circular plates used to press the permaglass rings against the aluminum ones⁶. This means that the pressure is distributed on three circular sectors (30° each), whose centers are 120° apart each from the others

In this configuration, gravity has not been applied, taking into account that, during the tests, data have been collected after having balanced the weight of the whole mounted assembly.

5.2 Type of analysis and Algorithm of solution: Non Linear vs Linear static analysis

Static analysis has been done to simulate the mechanical response of the detector model to several axial loads, with the aim of reproducing the tensile campaign measurements available for comparison.

As we can see in more details in the next paragraph, very low stress are produced in the detector when axial loads less than 3000 N are applied, so that the response of the detector is always in the elastic region. Consequently a simply linear static analysis is adequate to represent accurately the mechanical response of the model⁷ and estimate the

⁶The permaglass ring is in between the brass plates and the aluminum rings.

⁷We checked that, in these cases, it is not necessary to insert the curve $\sigma(\epsilon)$: in fact only the Young Modulus of the initial narrow linear region can be successfully used for each material, obtaining at the end the same results we get by the complete material behavior description, but with less computational effort.



Figure 21: Full detector mounted on the ENEA tensile Machine.

deformation to compare with the measurements available at the moment. A non linear static analysis is computationally more severe (essentially, from the cpu time point of view and disk usage) and is required either when large deformation are expected or when the material is brought to work in a region where the $\sigma(\epsilon)$ curve is no more linear.

However, non linear simulations (tensile load up to 30 kN) have been done to test they work properly, even if for validating them, we need to perform measurements with corresponding higher loads in the tensile tests. From the experimentally derived $\sigma(\epsilon)$ curves, we have, in fact, deduced that at least a 6kN load on all the assembly is required in order to leave the linear region. This new measurement campaign has been already scheduled at the beginning of 2010.

In the case of simulations of non linear static analysis (nlgeom), Newton-Raphson method has been used, activating for enhancing convergence the line search solution option (lnsrch,on).

6 Final Validation: experimental versus calculated deformations

Calculations have been done to simulate the mechanical response of the detector to axial tensile loads ranging from 100 up to 3000 N. Loads have been supposed to be applied



Figure 22: The extensometer used for elongation measurement

Load N	Measured U_z by extensometer [μm]	Calculated U_z by Ansys [μm]	Measures by comparators [μm]
100	11.58	20.24	10
500	57.91	101.	60
1000	115.82	202.4	110
1500	173.73	303.6	160
2000	231.63	404.8	-
2500	289.54	506	-
3000	347.45	607.2	-

Table 5: Comparison between measured and calculated values of axial elongation

slowly so that dynamic effects could be neglected. Only stationary analysis have been done up to now: linear and non linear ones. The variable to compare is the axial elongation U_z , estimated between the two permaglass rings: in table 5 the experimental and calculated values are reported. We measured the elongation using both the extensometer and a couple of comparators. Comparators are less precise respect to extensometer but allow us to have an absolute measurements. The two comparators have been placed in contact, respectively, with the lower and upper permaglass ring as shown figure 24.

According the measurements and in agreement with predictions , the detector works in linear region: the experimental data are well fitted by a line ($R^2 = 1$) of equation 1, while the calculated elongations may be fitted by a line ($R^2 = 0.999$) of equation 2:

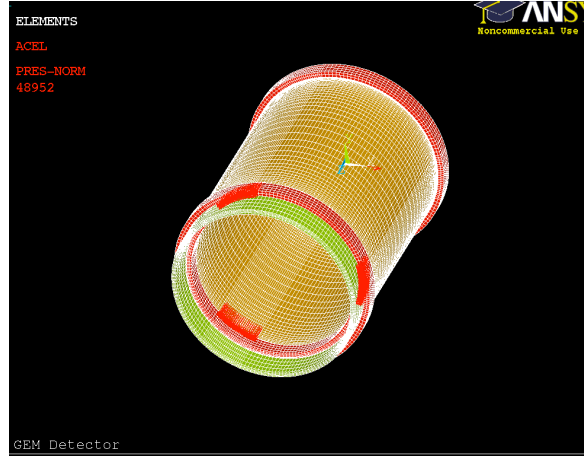


Figure 23: Load Applied: red arrows indicate uniform pressure on the permaglass ring portions in contact with the three brass plates

$$\textit{Measured } U_z[\mu\text{m}] = 11.58 \cdot 10^{-2} F[\text{N}] \quad F[0 \div 3\text{kN}] \quad (1)$$

$$\textit{Calculated } U_z[\mu\text{m}] = 20.24 \cdot 10^{-2} F[\text{N}] \quad F[0 \div 3\text{kN}] \quad (2)$$

The measurements done with the extensometer and the comparators are well in agreement and are a factor about 2 (exactly 1.77) lower than the estimated values by Ansys. The reason of this difference is still under investigation and could be due to a non precise characterization of the mechanical properties of the used materials or related to other causes.

One of the possible explanation could come from the permanent deformation, most probably due to buckling instability of thin cylinders under radial pressure, that the detector seems to be experienced after the tests with cooling gas, done at CERN, just before doing the tensile tests that we are describing in this report. In figure 25, we can see respectively, on the left, how the inner cylinder appeared to us, after having kept away the thin copper shield that had been used to protect the inner surface of the detector (without any structural task) and, on the right, the elastic buckling caused by an external overpressure (few mbar) on the outer cylinder, that we have caused by pumping out the air in the inner gap (between the Anode and the GEM3). The elastic buckling contrarily to the plastic one is visible only during load phase, and it disappears when loads stop to be applied.



Figure 24: Experimental set-up for measurements with comparators



Figure 25: On the left: plastic deformation of the Catode cylinder most probably due to buckling instability, caused by external gas pressure; On the right: elastic buckling on the outer cylinder due to an external radial overpressure.

7 Simulation Results of the tensile test at 1000 N on the detector prototype

We describe in detail the stress and strain fields that have been calculated for the prototype when 1kN tensile load is applied on it. This load corresponds to the prestress value that should be applied to the real detector, before setting it into operation around the Interaction Point of the DaΦne Layout. The results of the calculations refer to the tensile test configuration (i.e., gravity neglected and tensile load along the axis only).

7.1 Deformed shape

In figure 26 the total displacement has been shown for the whole detector. It consists essentially of an axial elongation with maximum value of 205 μm .

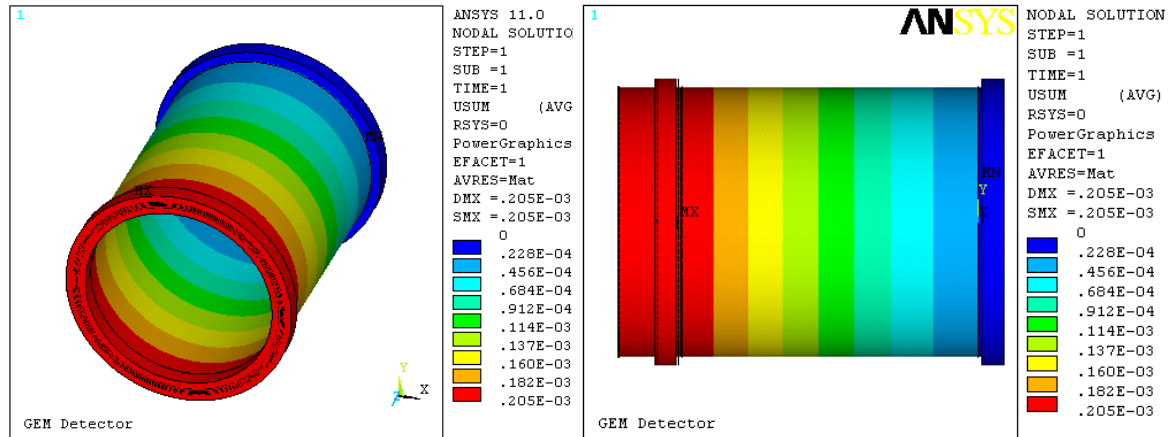


Figure 26: Total displacement (Nodal Solution). On the right the dotted lines are the undeformed edge of the detector. The displacement has been amplified by a factor 10 in order to be more visible

This means that all the GEM cylinders are stretched of the same quantity, causing a different level of stress in dependence on their own rigidity: because a higher value of the Young Modulus has been assigned to the Cathode, we expect it will be the most stressed one.

In figure 27, we reported the deformed shape of the detector around the permaglass rings. These regions appear to be the most critical ones since here the cylinders have lower rigidity due to the fact that the copper coating on each cylinder has been designed in such a way to leave a 5 mm strip of only kapton from the inner side of each permaglass ring (see figure 28). In these regions, high stress and strain gradients have been recorded as it will be discussed in the next paragraph.

The more flexible 5mm layers of only kapton on each cylinder take a “S shape”, shown in figure 29. This is because they connect more rigid structures radially displaced one respect to the other: on one side, the copper layered zone of each cylinder itself and, on the other side, the permaglass ring. In fact, because of the radial squeeze due to poisson coefficient, the copper layered zone of the cylinders tends to approach the central axis, while the permaglass rings are quite well fixed. This causes a shift in radial direction of the clumped extremities of the narrow kapton sheets that produces as a consequence the shown deformed shape.

Nearby the permaglas rings, the gap between the different cylinders is far away to

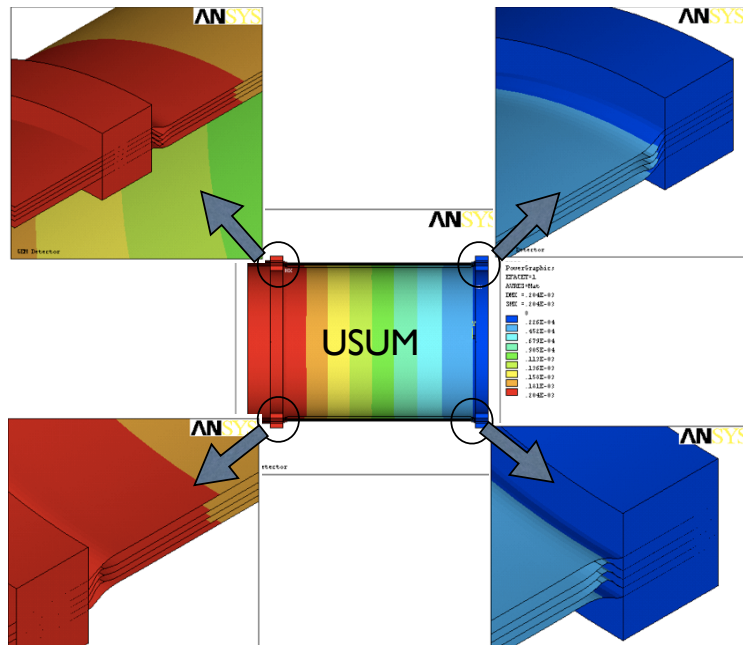


Figure 27: Cylinder deformation around the permaglass rings. Displacement has been amplified by a factor 100.

be uniform, but in the active zone (that is the zone where the cylinders are coated with thin layers of copper), the coaxial cylinders appear to preserve quite well the uniform distance one from the other, this being true when applied loads are in the range of only few kN. Even if the entity of these transversal displacements is little (about an order of magnitude less than axial displacement), indeed the cylinder regions around the permaglass rings appear to be, on the base of the previous considerations, the most critical ones.

7.2 Stress and Strain calculations

First of all we compared the nodal solution with the element one in order to understand if the discretization of the model is suitable in obtaining good accuracy in results: in fact a good mesh must produce solutions that in the two cases differ less than 10%. We remind briefly that in nodal solution the stress contours are averaged at the nodes, instead in the element solution data are unaveraged, showing discontinuity between elements. The difference between averaged and unaveraged stresses gives an indication of how “good” the mesh is (for an optimal mesh this difference reduces to a minimum value, trying to avoid to spend an huge amount of cpu time by increasing too much the element numbers).

In table 6 we reported the $\sigma^{gem}(act)$ and $\sigma^{max}(kap)$ for the averaged (nodal, “n”)

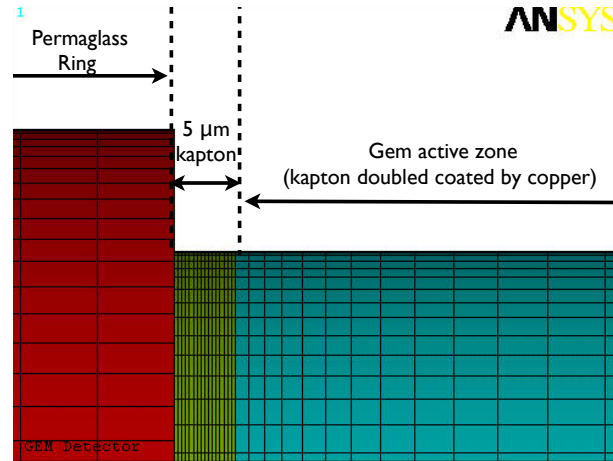


Figure 28: Schematic description of material distribution on each cylindrical layer of the detector

and not averaged (element, “e”) solutions: $\sigma^{gem}(act)$ indicates the uniform value in the active central zone of each cylinder, that is the zone where the kapton sheets are coated, whereas $\sigma^{max}(kap)$ is the maximum stress intensity reached in the narrow kapton zone of each cylinder, between the active zone and the inner surface of the permaglass rings (see figures 28 and 29).

As we can see in the table 6, the estimated average values of the stress on Anode, Catode and GEM cylinders are well in agreement with the unaveraged one, whereas the peak stress intensity differs by no more than 11% in the worst case, showing definitively the goodness of the obtained simulation results.

In order to reach such a good accuracy of results we needed to reduce the difference between element and nodal solutions in the critical zone of only kapton, where highest stress and strain gradients are located. This has been done by increasing the mesh density in these zones, and in particular the number of divisions in axial direction (16 in 0.5 mm) is a factor about 300 higher than the number of axial division in the active zone (40 in almost 400 mm). In any case also for the so called “active-gem-zone” (that is the double coated zone of the cylinder), we pay attention to distribute the mesh density in such a way to make the mesh more closely compacted near the borders, where we expect higher stress gradients, with respect to the central zone where the stress and strain are quite well uniform and constant (a mesh density ratio of about 20 has been applied, by means the “lesize” command, between external and central part of each cylinder generatrices in the active zone).

In figure 30 , 31 and 32 we reported the comparison between nodal and the element

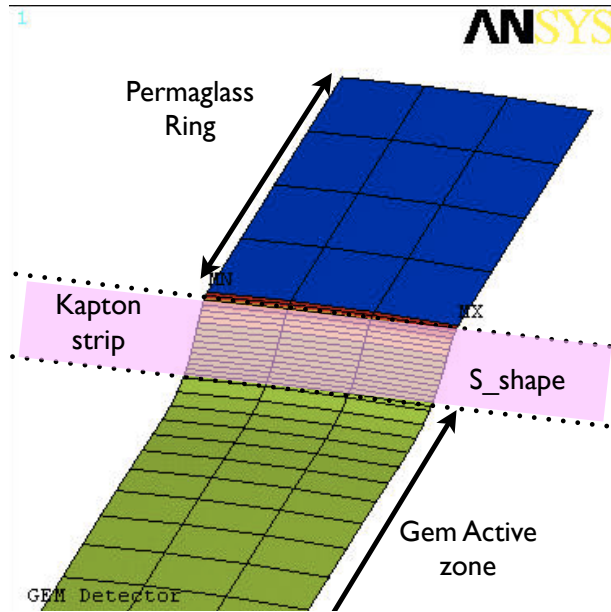


Figure 29: The “S” shape deformation of only kapton strips between permaglass ring and GEM active zone

Cylinder	$\sigma_n^{gem}(act)$ [MPa]	$\sigma_n^{max}(kap)$ [MPa]	$\sigma_e^{gem}(act)$ [MPa]	$\sigma_e^{max}(kap)$ [MPa]	$\epsilon(\frac{e-n}{(n+e)0.5})$ [%]
Anode	2.13	3.05	2.13	3.3	6%
Catode	3.3	4.0	3.3	4.34	8%
Gem1, Gem2, Gem3	2.69	4.1	2.69	4.6	11%

Table 6: Stress field calculation: comparison between Nodal and Element Solution

solutions respectively for Catode, Anode and GEM cylinders.

7.2.1 Analysis of the results for the GEM cylinders

The stress field on each GEM is shown in figure 32: even if this plot refers to GEM1 cylinder (the inner one), we can assert that it is representative of all the GEM cylinders, since an extremely little difference in stress intensity exists between them. An average stress value of about 2.7 MPa is uniformly present in the active zone (the double coated one), while the maximum stress gradients are in the only kapton zone (see figure 33). The maximum stress is about 4.1 MPa and is registered on the external stretched surface of each cylinder in correspondence of the border thickness attached to the permaglass ring

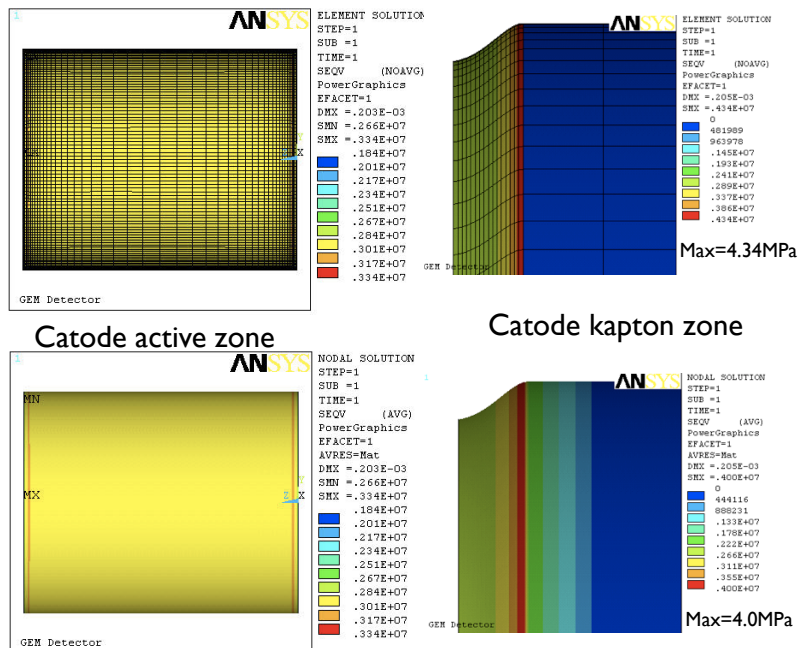


Figure 30: Comparison between nodal and element solutions for stress in Catode

(see figure 34).

In fact, because of the deformed shape, each cylinder is less stretched on the inner side respect to the external one (2.0 against 4.1 MPa), as better documented in picture 35; this means that cylinders experience also an important stress gradient in their thickness. In figures 36 and 37 we show, respectively, the transversal displacement and the total strain field, in one of the three GEM cylinders (exactly the external one, G3), taking in mind that the stress and strain fields are pretty well the same in the other two GEM cylinders. The maximum radial displacement is $40 \mu\text{m}$ and is reached along each generatrix at about 4.2 mm apart from the inner border of the permaglass ring, on both sides. The trend of the equivalent stress along each generatrix (cylindrical symmetry) is reported in figure 33: as we can see the stress is almost constant in the active GEM zone (central double coated), whereas it has a peak in the only kapton narrow region near the permaglass ring, where a maximum value of about 4.1 MPa is reached (that is 1.5 times the constant value in the double coated zone, 2.9 MPa). The stress intensity increases in very steep way inside the kapton strips, producing a stress gradient of about $(1\text{kPa}/\mu\text{m})$ along the axial direction (see figure 38).

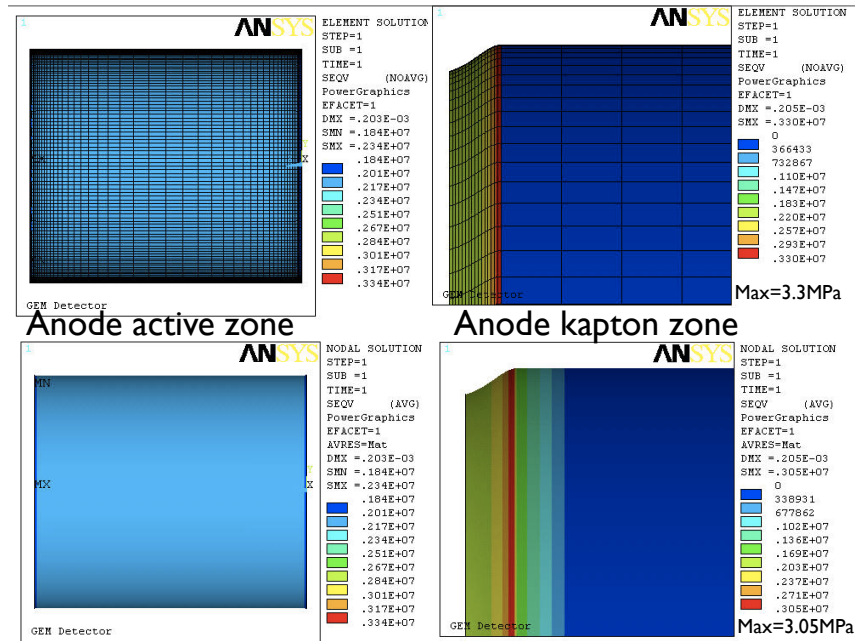


Figure 31: Comparison between nodal and element solutions for stress in Anode

7.2.2 Analysis of the results for the Catode and Anode

In figure 39 and 40, we reported, respectively, the equivalent stress and the radial displacement U_r , along a generatrix, for both Anode and Catode cylinders (the stress and the radial displacement fields have both a cylindrical symmetry). Catode appears to be more stressed in the active zone with respect to Anode of about a factor 1.5, corresponding quite well to the ratio “Catode Young Modulus /Anode Young Modulus”⁸. As a consequence, Catode, being more rigid, tends to be less deformed and in the case of equal axial displacement it is more stressed than the other cylinders.

We conclude reporting in figure 41 and 42, the comparison of the stress and transversal deformation on all the different cylinders (taking in mind that the axial deformation is the most important one and it is equal for all the cylinders).

8 Future Plans and Conclusion

In this report, we described the tensile test campaign carried out on Anode, Catode and GEM specimens, thanks to which we could define the $\sigma(\epsilon)$ curve for each material. These

⁸In the first linear region of the $\sigma(\epsilon)$ curves the young modulus ratio corresponds respectively to $(5.29GPa/3.74GPa) \simeq 1.4$.

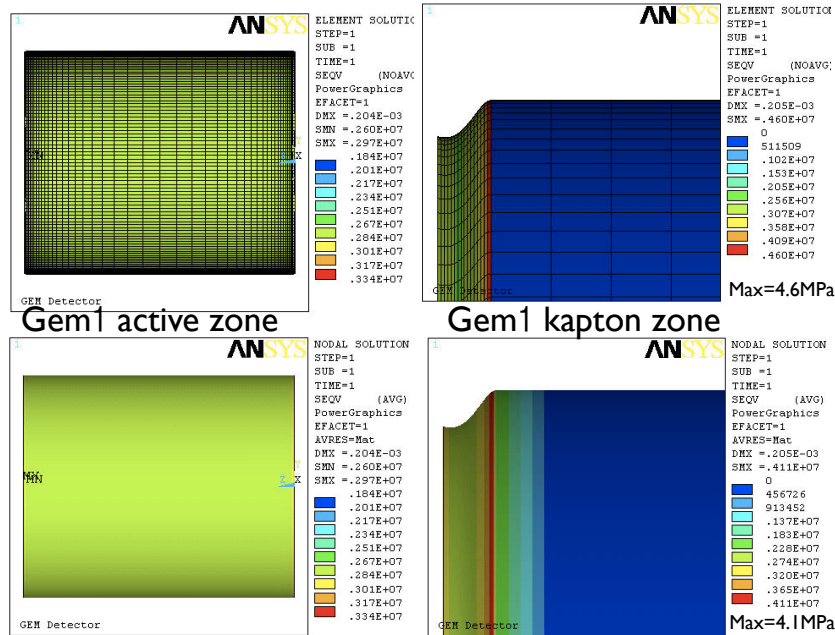


Figure 32: Comparison between nodal and element solutions for stress in GEM

measurements are of fundamental importance in defining the elasticity parameters of all those non conventional materials used to build the detector. The experimental data have been properly used in the input data file of Ansys code, by which we realized the finite element model of the whole cylindrical detector prototype.

The main aim of realizing a finite element model by Ansys consists in making available a mathematical tool that allows to do predictions about static and dynamic response of the detector to different load and boundary conditions.

The mandatory step to accomplish, in order to understand the actual reliability and accuracy of the finite element model, was to validate the simulation results against experimental values, collected during the tensile test campaign realized on the detector prototype at the ENEA mechanical workshop in Frascati. In particular we measured the axial elongation of the whole assembly under well known tensile loads.

The comparison between experimental values and simulation predictions showed that the elongations estimated by Ansys are a factor almost 2 larger than those measured.

Some hypothesis have been formulated concerning the main causes of this difference and several investigations are currently in progress. The most probable cause could be the buckling plasticization that we discovered on the inner cylinder (Catode), once the

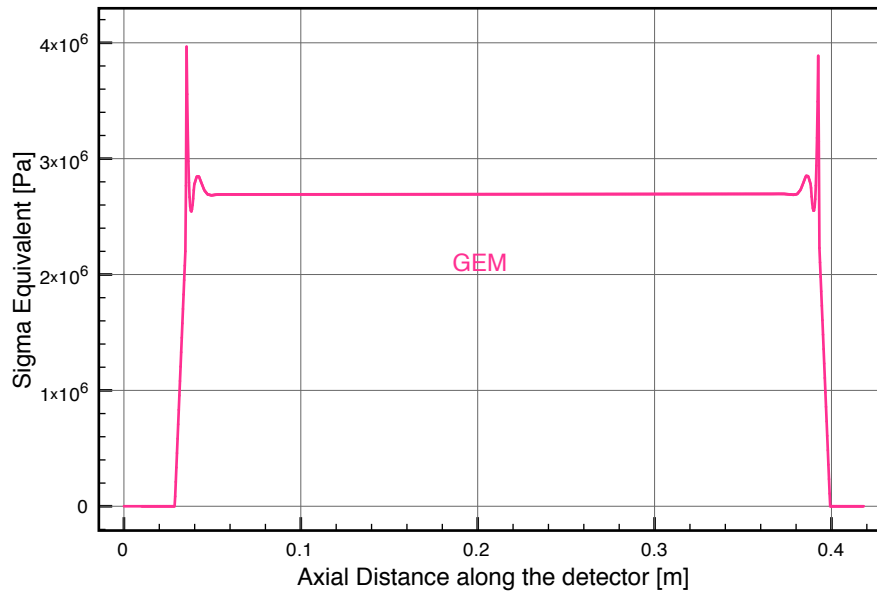


Figure 33: Equivalent Stress (σ_{eq}) curve along detector for GEM cylinders

electronic inner shield had been removed⁹. This plasticization can be correlated, very likely, to the gas flowing through the detector, during the tests conducted at CERN, in Geneva. In fact an external radial over-pressure could have generated a buckling instability on the stretched cylinder, causing as a consequence an alternating distribution of convex and concave lateral surface deformation.

In the last part of the report we discussed the results of the simulation (by Ansys code) of the static response of the detector prototype to a tensile load of 1 kN: in particular, the stress and strain fields on all the cylinders have been estimated. The results show that from the structural point of view the most critical region appears to be the narrow strip of only Kapton on each cylinder: in fact very large stress and strain gradients have been calculated in this zone. In any case when a tensile load of 1 kN is applied, the maximum stress does not exceed 4 MPa, that means the detector operates everywhere in the elastic region of the curve $\sigma(\epsilon)$.

To conclude, the future plan of this study can be summarized in the following items:

- To perform analysis of buckling instability on Anode, Catode and GEM cylinders in order to understand what is the minimum critical overpressure that could cause

⁹We have to point out that during the tensile tests on the whole prototype, the maximum load applied was 3kN, remaining far away from plasticization.

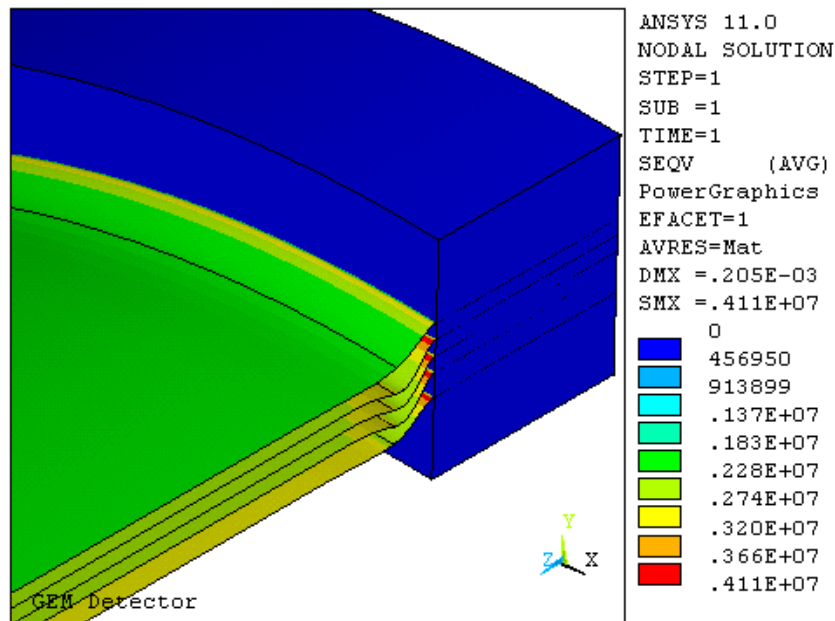


Figure 34: Maximum stress location in the GEM detector

buckling plasticization as a function of the tensile stress.

- To perform Ansys simulations on the real cylindrical detector in working configuration on the DaΦne interaction Point, in presence of gravity, to estimate the optimal tensile test to apply in order to reduce the mechanical transversal deformation, preserving the cylindrical symmetry.

References

- [1] <http://www2.dupont.com/Kapton/>
- [2] D. Y. W. Yu et F Spaepen “*The yield strength of thin copper films on Kapton*”, Journal of Applied Physics, vol 95, Number 6.
- [3] <http://www.ansys.com/>

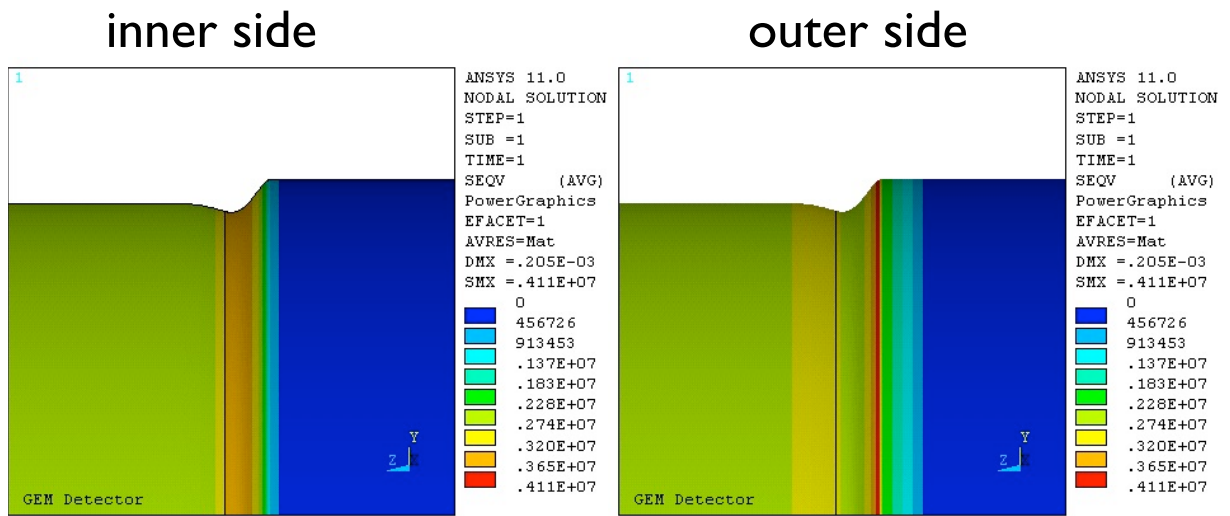


Figure 35: GEM Stress Gradient detail: on the left, stress gradient in the inner face and on the right stress gradient on the external face of the GEM cylindrical foil

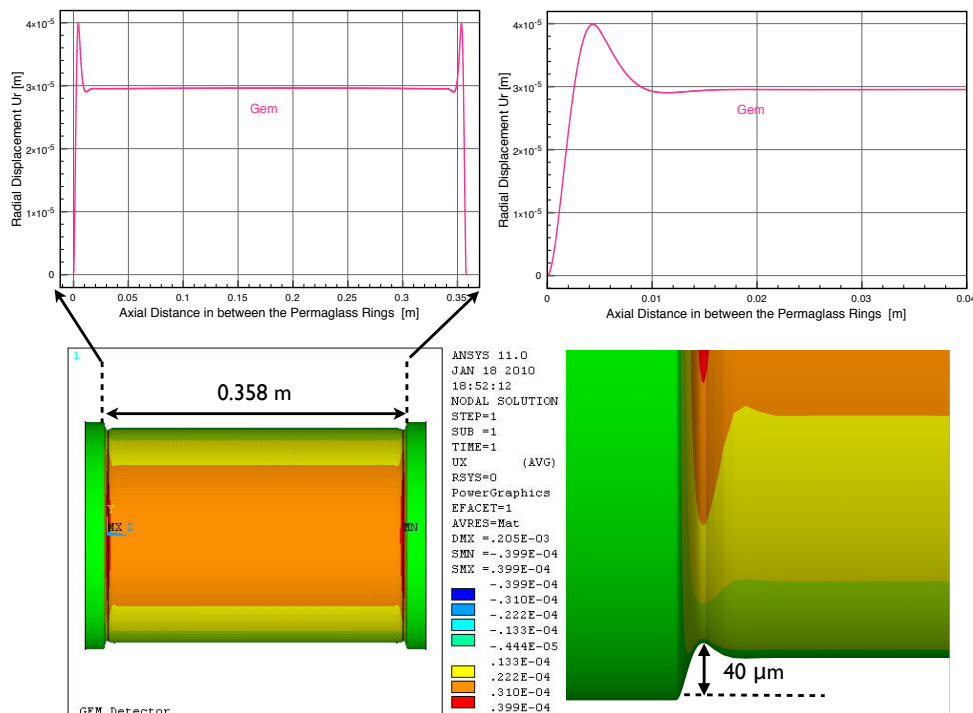


Figure 36: Gem Transversal Deformation (U_r); Displacement has been amplified of a factor 100.

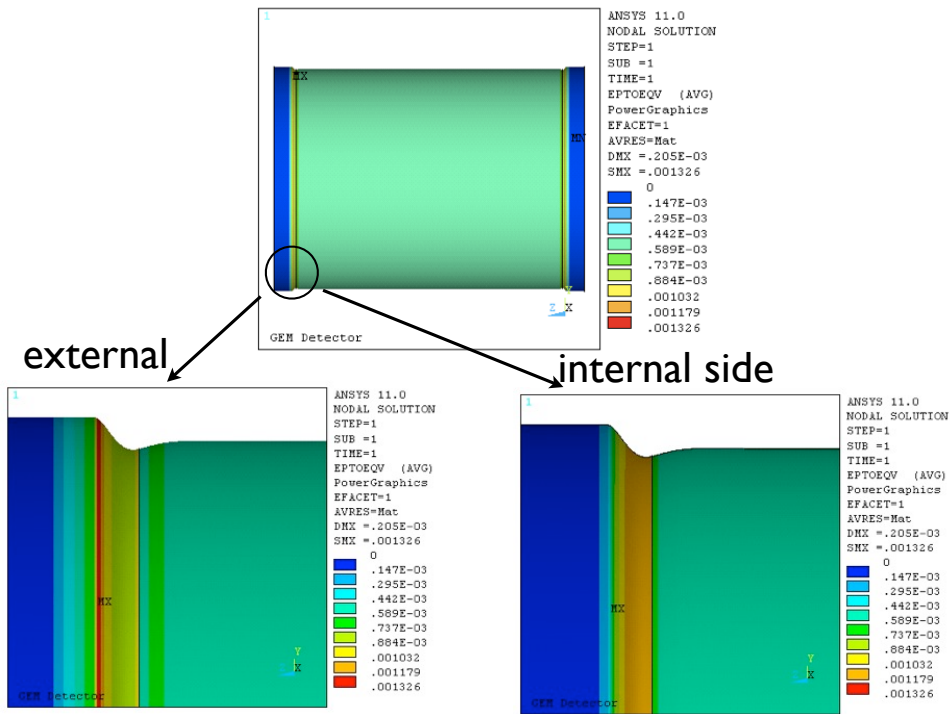


Figure 37: Gem Strain Field

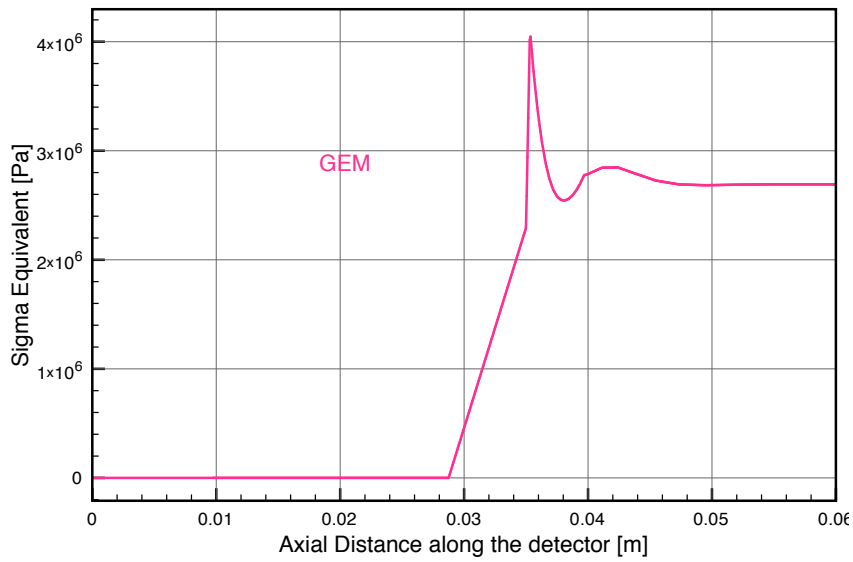


Figure 38: Gem Stress Curve Detail

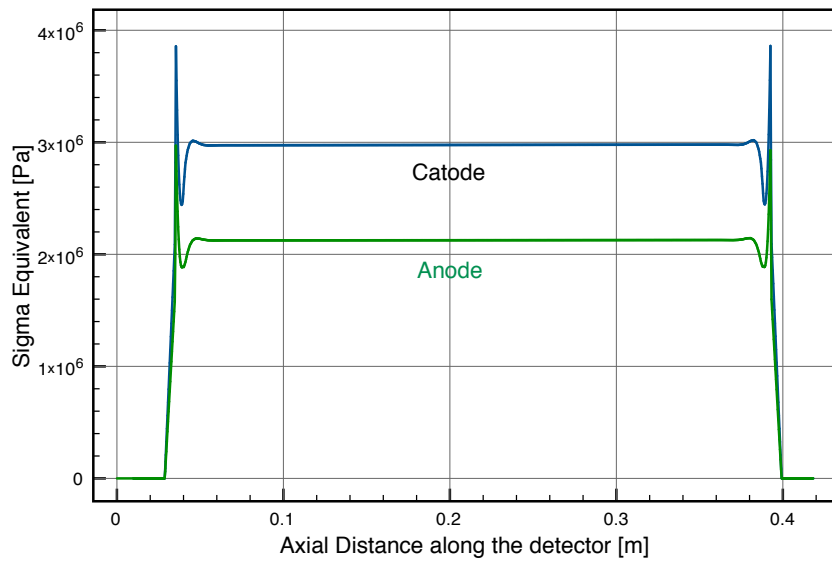


Figure 39: Equivalent Stress curves along generatrix for Anode and Catode.

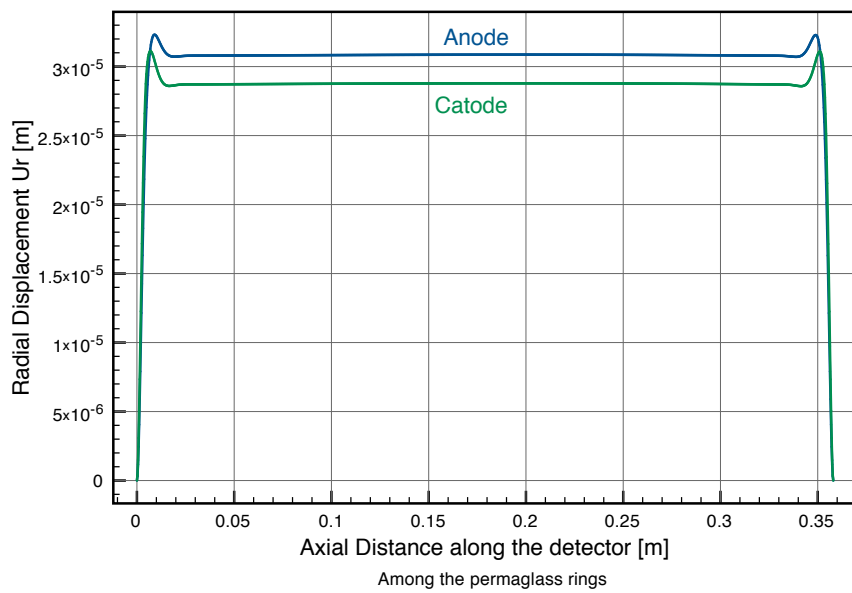


Figure 40: Radial Displacements (U_r) for Anode and Catode

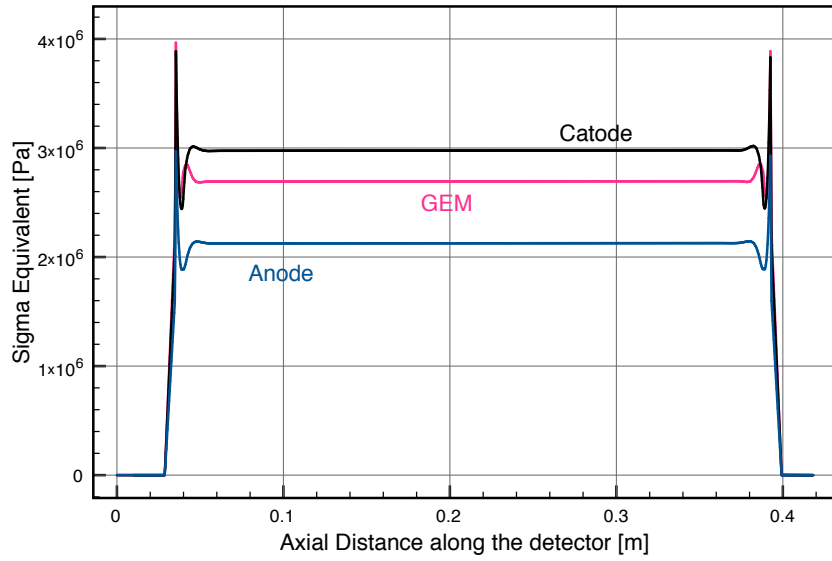


Figure 41: Comparison between the stress curves, along a generatrix, of Anode, Catode and GEM cylinders.

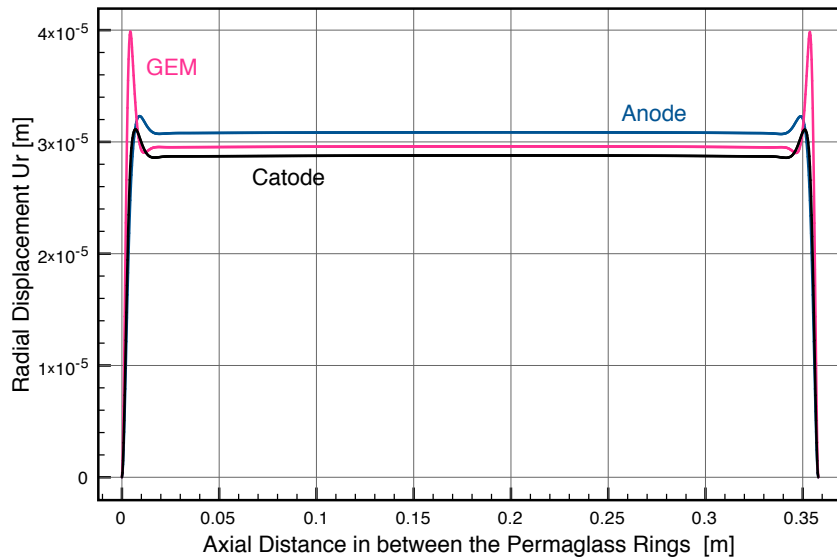


Figure 42: Comparison between the Radial Displacements (U_r), along a generatrix, of Anode, Catode and GEM cylinders.